Proceedings of the XI DINAME, 28th February-4th March, 2005 - Ouro Preto - MG - Brazil
Edited by D.A. Rade and V. Steffen Jr.

DYNAMICAL RESPONSE OF MISALIGNED AND CRACKED ROTORS

Dr Pedro N. Saavedra
Facultad de Ingeniería. Universidad de Concepción. Chile
e-mail:psaavedr@udec.cl

Msc Daniel Ramirez
Facultad de Ingeniería. Universidad de Concepción. Chile
e-mail:danirami@udec.cl

Abstract. *In this work a theoretical and experimental analysis of two misaligned rotor-bearing system connected by a flexible coupling and a rotor- bearing system with a transversely cracked shaft are presented. Based on tests on coupling stiffness, a new coupling finite element stiffness matrix has been deduced. This has been used in the finite element analysis of a two-rotor system connected by a flexible coupling, to calculate the mechanical vibration resulting from mixed angular and parallel shaft misalignments with residual unbalance. The vibration generated is of the parametric type, and it is caused by variation in the coupling stiffness as the shaft rotates. As a consequence, the vibration spectral response is directly related to the spectral coupling stiffness, i.e., it is strongly dependent upon the type of coupling used. In order to model the cracked shaft for FEM analysis, a finite element for a cracked cylindrical shaft is developed. The additional flexibility due to the crack is evaluated from the linear fracture mechanics, using a breathing crack model derived in a rigorous way. The resulting parametrically excited system is non-linear and the equations of motion are solved using Hilbert, Hughes and Taylor integration method (HHT) implemented in Matlab platform. The theoretical results are compared with those obtained on a test rig. Good agreement between them is obtained.*

Keywords *:rotor vibration analysis, condition monitoring*

1. Introduction

In all industries around the world, maintenance strategies are changing from periodic inspection strategies to condition-based, predictive maintenance strategies. Condition monitoring can improve the availability of machinery by being able to pinpoint and diagnose problems at an early stage while the machinery is working. This process avoids offline inspections with consequent loss of production, and reduces unplanned downtime. Vibration analysis is certainly one of the most powerful methods in current use in machinery diagnosis.

However, there is a lack of research on the ultimate objective of diagnostic techniques, which is the determination of reliable vibratory indicators to differentiate between problems that exhibit similar frequency spectra and waveform vibrations. Examples are, shaft misalignment and cracked shafts. The importance of discriminating between these problems can be seen in that, in the first case, the machinery must be stopped as soon as possible to avoid a catastrophic failure, and in the second case, the machinery can usually wait for the next scheduled maintenance period. Thus, to develop a reliable diagnosis, a thorough understanding of the physics of the problem and its effect on machine vibration is necessary. The work presented in this paper describes theoretical and experimental work on the vibration behaviour of coupled rotors with flexible couplings and the vibration behaviour of a rotor with a cracked shaft.

2. Misaligned rotor coupled through a flexible coupling

Shaft misalignment is one of the most common causes of vibration in rotating machinery. Shaft misalignment is defined as the deviation of the shaft position relative to a collinear axis of rotation measured at the points of power transmission between two machines. Shaft misalignment generates additional loads on bearings, seals, shafts, and couplings, so decreasing their operating lives, and when it is excessive, shaft misalignment can induce early failure,

To investigate the effect of misalignment on the behaviour of rotor vibration, a simple but general dynamic model system, as illustrated in Fig. 1, will be analysed. This consists of two rotors connected by a flexible coupling. Each bearing rotor system comprises of a set of interconnecting components consisting of rigid disks, shaft segments with distributed mass and elasticity, and two antifriction-type bearings.

The components are discretized by the finite element scheme, as shown in Fig. 1. The eight black dots indicated are the numbers of the nodes utilized. We considerer five degrees of freedom for each node u_i , v_i ,w_i, , θ_x^i , θ_y^i , where u_i, v_i, and w_i are the node displacements in the x-, y-, and z-axis directions, respectively, and θ_x^i and θ_y^i are the rotations about the x- and y-axes, respectively.

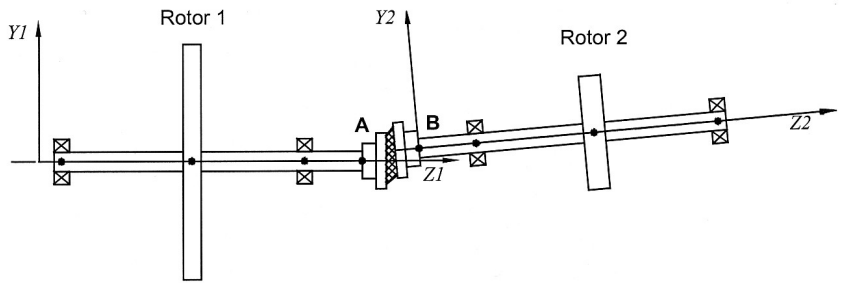

Figure1. Schematic drawing of two misaligned rotors

2.1. Coupling element

A coupling stiffness matrix is constructed to include the coupling element in the finite element analysis. For this purpose, we consider the coupling element as a couple of rigid blocks, joined together by an elastic element.. The elastic element is characterized by five springs: three linear springs along the z-axis (axial), x-axis (transversal), and y-axis (transversal), respectively, and two bending springs in the yz-plane (x-axis rotation) and in the zx-plane (y-axis rotation), respectively. Each of these five springs has its own associated stiffness coefficient, namely, K_a, K_{tx}, K_{ty}, K_{fx}, and K_{fy}. As manufacturers do not publish these stiffness coefficients, they must be determined by experiment. Figure 2 shows the results of the test obtained for K_t for the Paraflex and three jaws couplings respectively.

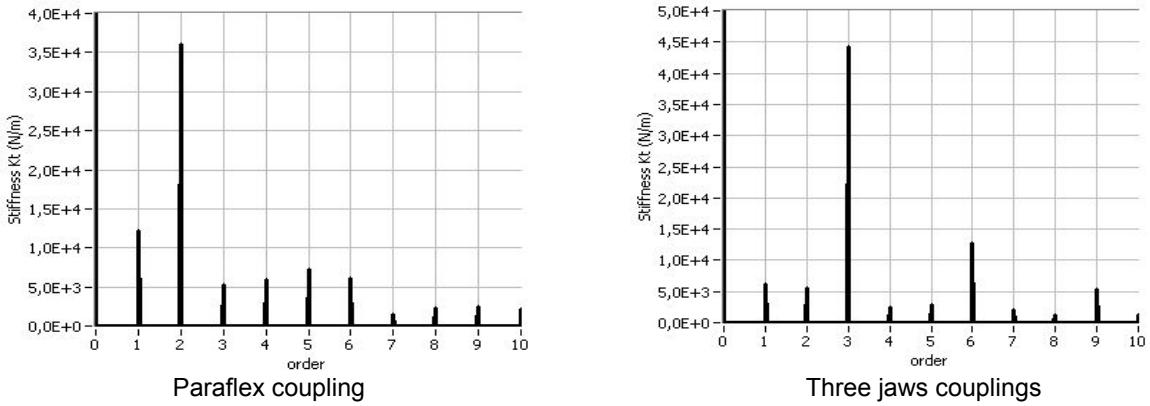

Figure 2. Transverse stiffness spectrum for the Paraflex and three jaws couplings

In general, the stiffness coefficients, K_i, for a specific flexible coupling type depend upon the rotation angle, α, the transmitted torque, T, the rotation speed, Ω, the magnitude of misalignment horizontal and vertical displacements, , δ_x and δ_y, and the magnitude of the misalignment angles, φ_x and φ_y. Being the rotational angle the main factor, in this work, it is considered that the stiffness coefficients only depend on it.

$$\mathbf{K}^c = \begin{bmatrix}
K_{tx} & & & & & & & & & & \\
0 & K_{ty} & & & & & & & & & \\
0 & 0 & K_a & & & & & & & & \\
0 & -K_{ty}\frac{L}{2} & 0 & \left(K_{ty}\frac{L^2}{4}+K_{fx}\right) & & & & & & & \\
K_{tx}\frac{L}{2} & 0 & 0 & 0 & \left(K_{tx}\frac{L^2}{4}+K_{fy}\right) & & & & & & \\
-K_{tx} & 0 & 0 & 0 & -K_{tx}\frac{L}{2} & K_{tx} & & & & & \\
0 & -K_{ty} & 0 & K_{ty}\frac{L}{2} & 0 & 0 & K_{ty} & & & & \\
0 & 0 & -K_a & 0 & 0 & 0 & 0 & K_a & & & \\
0 & -K_{ty}\frac{L}{2} & 0 & \left(K_{ty}\frac{L^2}{4}-K_{fx}\right) & 0 & 0 & K_{ty}\frac{L}{2} & 0 & \left(K_{ty}\frac{L^2}{4}+K_{fx}\right) & & \\
K_{tx}\frac{L}{2} & 0 & 0 & 0 & \left(K_{tx}\frac{L^2}{4}-K_{fy}\right) & -K_{tx}\frac{L}{2} & 0 & 0 & 0 & \left(K_{tx}\frac{L^2}{4}+K_{fy}\right)
\end{bmatrix}$$

The stiffness matrix of coupling element $\mathbf{K^c}$ used in this paper is that one developed by Ramirez (2003),as is indicated above. This 10x10 matrix relates the forces $\mathbf{P^c}$ and displacements $\mathbf{d^c}$ on the coupling end nodes A and B.

The equation of motion for the coupling element using the previously defined stiffness matrix is:

$$\mathbf{M^c\ddot{d}^c + K^c(\alpha)d^c = P^c} \tag{1}$$

where the mass matrix is conformed by two discrete masses at the coupling nodes with values equal to the hub's mass.

In Fig. 1 Z1 and Z2 denoting shaft centrelines connected by a flexible coupling. For practical reasons, we define one reference system for each rotor as X1Y1Z1 and X2Y2Z2, respectively. For the assembling procedure of all the system elements, the appropriate node displacement vectors must refer to the correct reference system that the nodes belong to. The nodes of the shaft, disk, and bearing elements belong to the same reference system, but the coupling element has one node belonging to one reference system, and another node belonging to the second system. Because of this, the motion equation of the coupling element, Eq. 1 defined for one reference system, must be changed by coordinate transform in such a way that the displacements for nodes A and B be referred to coordinate system X1Y1Z1 and X2Y2Z2, respectively.

Equation 1 can be split in two subsystems:

$$\mathbf{M_u^c\ddot{d}_1^c + K_u^c(\alpha)d_1^c = P_1^A} \tag{2}$$

$$\mathbf{M_l^c\ddot{d}_2^c + K_l^c(\alpha)d_2^c = P_2^B} \tag{3}$$

The sub indices “1” and “2” refer to the X1Y1Z1 and X2Y2Z2 coordinate systems, respectively, so that $\{d_1^c\}$ is a 10 x 1 vector displacement of the coupling with reference to the X1Y1Z1 system, and $\{d_2^c\}$ is a 10 x 1 vector displacement of the coupling with reference to the X2Y2Z2 system. The subindices “u” and “l” refer to the upper and the lower half of the stiffness and mass 5 x 10 matrices. The vectors d_1^c and d_2^c contain the displacements of both nodes in reference to the same system, and, as it was indicated previously, the displacements for node A must be referred to the X1Y1Z1 system, and the displacements for node B must be referred to the X2Y2Z2 system.

Following the developing of Ramirez(2003) it arrive to:

$$\mathbf{M^c\ddot{d}^c + K^c(\alpha)d^c = P^c + P^c_{misal}} \tag{4}$$

where

$$\mathbf{P^c_{misal} = K^c_L(\alpha)}\begin{Bmatrix} d_{0B} \\ \mathbf{0} \end{Bmatrix} - \mathbf{K^c_U(\alpha)}\begin{Bmatrix} \mathbf{0} \\ d_{0B} \end{Bmatrix} \tag{5}$$

$$\mathbf{d_{0B} = \left[\delta_{xB} \quad \delta_{yB} \quad \delta_z \quad \varphi_x \quad \varphi_y\right]^T} \tag{6}$$

P^c_{misal} is the loads generated by the misalignment on the coupling nodes, P^c is the forcing vector for the coupling element, K_U^c and K_L^c are the upper and lower halves of the stiffness matrix, respectively and d_{0B} is the initial misalignment vector measured in node B of the coupling. The magnitude of the misalignment displacement, δ_x, δ_y, and δ_z, and the magnitude of the misalignment angles, φ_x and φ_y, can be computed using the values and directions of the displacements obtained from a graphical plot of the reverse indicator readings in a similar way to the calculations made by Gibbons (1976).

From Eq.(4) it can be seen that loads generated by misalignment are directly proportional to magnitude of misalignment and the coupling stiffness. An important practical conclusion can be drawn from this: if the magnitude of misalignment increases, then the vibration amplitude will increase if the coupling stiffness increases or stays constant with increasing magnitude of misalignment. More misalignment means more vibration, more bearing overload, and shorter bearing life. That is, the measurement of vibration is a good indicator for detecting misalignment in machinery that is running, and for evaluating the severity of misalignment. This statement is not always true if the stiffness decreases with increasing magnitude of misalignment.

2.2. Equations of motion of the system

Assembling the equations of motion for the shaft, disc, bearing, and coupling elements, a finite element model suitable for simulating the dynamic response of misaligned rotors is obtained, where **M**, **K** and **C** are the mass, stiffness and equivalent damping matrix of the whole system , **d** is the displacement vector of the system and **P** is the external

forces on the system included the misalignment force. The model allows us to introduce all types of shaft misalignment and all types of flexible coupling.

$$\mathbf{M}\ddot{\boldsymbol{d}} + \mathbf{C}\dot{\boldsymbol{d}} + \mathbf{K}\boldsymbol{d} = \boldsymbol{P} \tag{7}$$

The equation of motion shown in Eq.(7), was solved numerically using Newmark's integration method, to obtain the steady state vibratory response of a system using the three jaws couplings for various operation speeds and different combined misalignments. Figure 3 shows the spectrum of the steady state response at inboard bearing of the motor in the x-direction with $\delta_x = -0.35$ mm and $\varphi_y = 0.105^o$. It can be seen that the main component of the vibratory spectrum is order = 3, which is the same as in the K_t spectrum, Fig. 2. The similarities between the K_t spectrum and steady state response spectrum are repeated in most of the simulation results. The results from the numerical simulations are in agreement with previous qualitative analyses, showing that vibration generated in misaligned shafts is caused by the variation in coupling stiffness with rotation angle, α, and that the frequencies of the steady vibratory response are the same as the stiffness coefficients, showing similar spectral patterns.

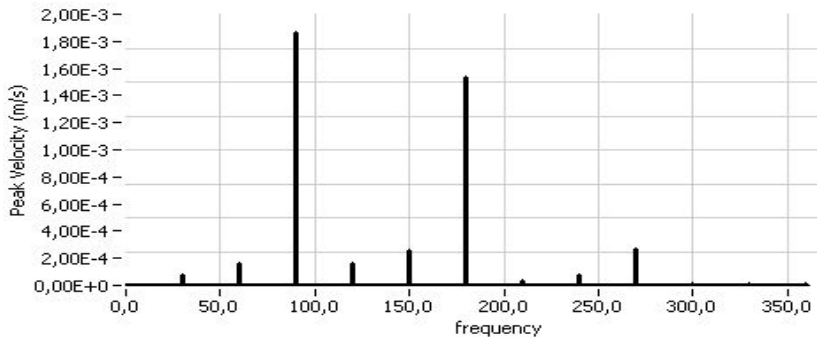

Figure 3.Vibration response for a three jaws coupling in the x-direction.

2.3. Experimental results

Laboratory tests were performed to confirm the theoretical model developed. The experimental rotor system used in this work was composed of a motor and a generator, which were connected by commercial couplings. Two commercial flexible couplings were used in the experiments:, three-jaw Lovejoy, and Paraflex couplings. The motor was an asynchronous, induction-type, with two poles and a frequency converter to feed it. The generator was a DC-type, and the resistant torque was determined from the electrical resistance of the armature coil and the DC excitation applied to field coil. The generator mounting allowed for arbitrary displacements on the supports. Therefore, the operating speed, resistance torque, and degree of misalignment could be easily controlled.

Special care was taken to avoid any undesirable problems, such as soft footings, distorted cases, and other faults that could introduce foreign dynamic effects. The measurement instrumentation included accelerometers, displacement probes, a photo-tachometer, a modal testing hammer, and a PC with data acquisition boards. The acquisition boards could simultaneously record eight data inputs for further processing.

In the theoretical study of the problem, it was concluded from Equation (4) that loads generated by misalignment are directly proportional to degree of misalignment and the coupling stiffness. To study this experimentally, the effect of the degree of misalignment on the vibration spectrum was examined. The initial experimental shaft alignment was carefully achieved using the reverse indicator method, Piotrowski (1986). Then, the aligned system was used as a reference for introducing the desired shaft misalignment. The measured frequency spectra of the horizontal vibration on the inboard bearing of the motor for different degrees of misalignment are shown in the cascade diagram of Fig 4 for the Paraflex coupling. These experimental results show that the shape of the vibration spectrum under the same misalignment conditions depends on the type of coupling used. This is contrary to what Xu and Marangoni (1994) indicate, who state that two different flexible couplings exhibit similar frequency characteristics in their vibration spectra when they are under the same misalignment and unbalance conditions. The experimental results also show that the magnitude of the spectral components is dependent on the magnitude of the misalignment.

If a specific frequency component of the vibration response is at, or close to one of the system's natural frequencies, then a resonance condition occurs, and its amplitude will be amplified and can become the largest component of the measured frequency spectrum. On the other hand, if the component is in a spectral zone where the mechanical mobility is low, then the amplitude of the component will be decreased. For the test rig results, the first natural frequency is at f = 63 Hz. Figure 5 shows the horizontal vibration spectra measured on the inboard bearing of the motor for two shaft rotation speeds. It can be clearly seen that the major components in the spectra are those that they are within the resonant zone of the system.

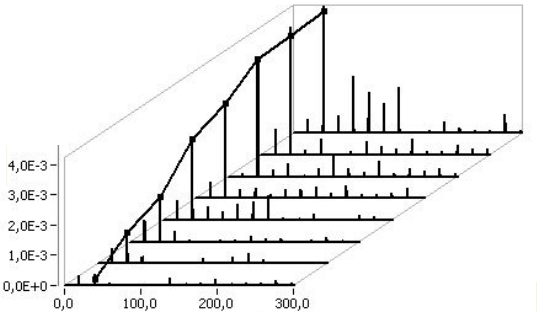

Figure 4. Vibration spectra of the Paraflex coupling

Previous works have tried looking for which harmonic of the shaft's running speed had the highest amplitude in the spectrum on misalignment shaft. This has been considered to be the best indicator for diagnosing shaft misalignment for a given coupling. Figure 5 illustrates that this approach is erroneous. It can be seen that in this case, any harmonic of the rotational speed can become the highest component.

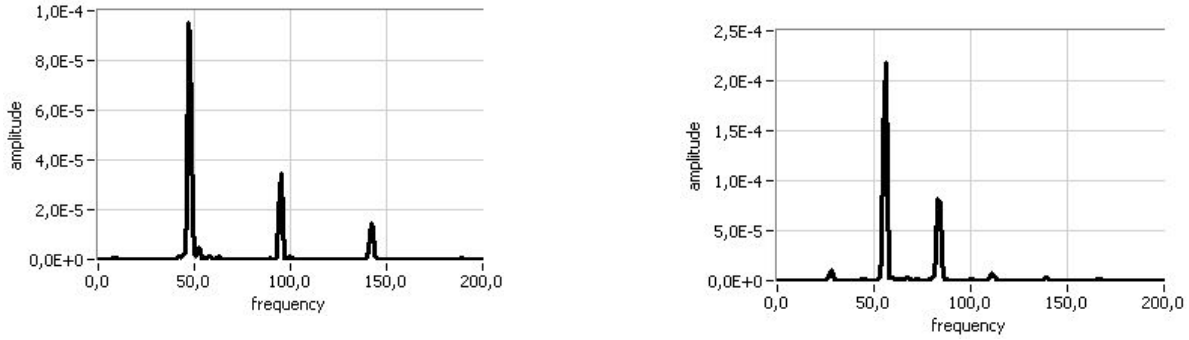

Figure 5. Vibration measurement at two rotational speeds: 48 and 28 Hz

This paper reveals the following conclusions that are useful for identification of shaft misalignment and its diagnosis using vibration analysis in the case of flexible couplings.

1. The frequency spectrum is composed of a series of harmonics of the running speed.
2. The system spectral amplitudes are directly related to the spectral amplitudes of the coupling stiffness, and so to carry out a reliable diagnostic, it is necessary to know the stiffness spectrum of the coupling used. Generally, for symmetrical couplings, the components at a connection multiplied by the shaft speed, and its harmonics dominate the vibration spectra.
3. If one spectral component is at, or close to, a system's natural frequency, then it will be amplified, and can dominate the spectrum.
4. In general, spectral amplitudes in the vibration spectra are proportional to the magnitude of misalignment. This allows us to evaluate the severity of shaft misalignment when monitoring the vibration spectrum. The measurements
5. Shaft misalignment generates vibration in two connected machines. This is used in the field to differentiate shaft misalignment from other faults that generate similar spectra. However, if the vibration is present on a single machine, this could indicate a cracked shaft.

3. Cracked rotor

One of the most serious problems in rotating machinery is the catastrophic failure due to presence of a crack. Although, the machinery are minutely inspected before their start-up and during their operation life, there are records of catastrophic failure due to the collapse of cracked shafts. Although the problem of cracked shaft is very important and there's plenty of literature about it, there is a lack of research concerning the ultimate objective of diagnostic techniques, which is to determine reliable vibratory indicators to differentiate a cracked shaft from other problems that present similar frequency spectra and waveforms vibration, such as a shaft misalignment. Thus, to develop a reliable diagnostic, a thorough understanding of crack behavior and its effects to a machine vibration is necessary.

In the analytical study of this problem the crack model is taken as the basic element. A crack introduces local flexibility to a shaft. The cracked section subjected to the internal forces P_1, P_2, P_3, P_4, P_5 and P_6, shown in Fig.6,

produces local additional displacements u_i between the right and left sections of the crack, in a similar way as an equivalent spring. These displacements u_i, in the i direction, under the action of the force P_i are given by the following expression, according to Castigliano's theorem:

$$u_i = \frac{\partial}{\partial P_i}\int_0^a I(\alpha)d\alpha \tag{8}$$

where $I(\alpha)$ is the strain energy density function, Dimarogonas and Papietiis (1983)

The additional flexibility introduced due to the crack is obtained combining Eq. (8) and the definition of the flexibility, Eq. (9):

$$C_{ij} = \frac{\partial u_i}{\partial P_j} = \frac{\partial^2}{\partial P_j \partial P_i}\cdot\int_0^a I(\alpha)d\alpha \tag{9}$$

The stress intensity factor depends on the geometry of the crack, the cross-section and the load that acts on it. They are calculated from the values of Kij known in the literature Saavedra et al. (1996)

3.1 Cracked beam finite element

In this work, an improved finite element model for a cracked shaft is shown and it is used in a finite element formulation to study dynamic behaviour of a test rotor, which is affected by the presence of a crack in the shaft. The direct and the cross-coupled stiffness are calculated by lineal fracture mechanics concepts, considering the partial opening and closing behaviour of a breathing crack. thus a cracked finite element matrix is described. The theoretical results are compared to experimental results.

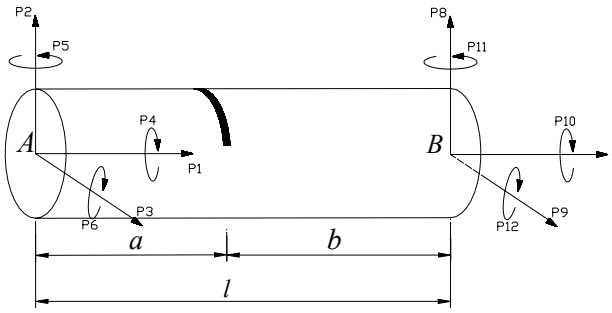

Figure 6. Schematic cracked finite element.

The crack is located a distance a from the left end of the element, Fig. 6, and the displacement of both transverse section of the crack are determinate by the vector u_L and u_R, where L and R refer to the left and right sections respectively

The relation of the relative displacement between both sections is:

$$\mathbf{u_R} - \mathbf{u_L} = \mathbf{C^1}\cdot\mathbf{P_R} \tag{10}$$

where $\mathbf{C}^1$ is the additional flexibility matrix that the crack introduces, and $\boldsymbol{P}_R$ is the force vector that acts in the right section of the crack. In addition, the displacement of node B can be expressed in terms of the load applied in B and of the displacement in R.

$$\mathbf{u_B} = \mathbf{C_b^0}\cdot\mathbf{P_B} + \mathbf{A}\cdot\mathbf{u_R}$$
$$\Rightarrow \mathbf{u_R} = \mathbf{A^{-1}}(\mathbf{u_B} - \mathbf{C_b^0}\cdot\mathbf{P_B}) \tag{11}$$

Matrix $\mathbf{A}$ is obtained from the relative displacements of point R in respect of node B and $\mathbf{C}_b^0$ is the flexibility matrix of a non-cracked element of length b. On the other hand, the u_L displacement can be expressed as a function of $\mathbf{C}_a^0$, which is the flexibility matrix of a non-cracked element of length a :

$$\mathbf{u_L} = \mathbf{C_a^0} \cdot \mathbf{P_L} \tag{12}$$

Matrix *B* can be obtained from the equilibrium conditions:

$$\mathbf{P_R} = -\mathbf{B} \cdot \mathbf{P_B} \qquad \mathbf{P_L} = -\mathbf{B} \cdot \mathbf{P_B}$$

and substituting into Eq. (11), u_B becomes:

$$\mathbf{u_B} = \left[\mathbf{B^T} \cdot \left(\mathbf{C_a^0} + \mathbf{C^1}\right) \cdot \mathbf{B} + \mathbf{C_b^0}\right] \cdot \mathbf{P_B}$$

Therefore, the flexibility matrix of a crack element yields:

$$\mathbf{C_c} = \mathbf{B^T} \cdot \left(\mathbf{C_a^0} + \mathbf{C^1}\right) \cdot \mathbf{B} + \mathbf{C_b^0} \tag{13}$$

To determine a cracked element stiffness matrix, as it is shown in Fig. 9, the following procedure is carried out. Considering the relative displacements of node *A* in respect of node *B* as:

$$\mathbf{P_B} = \left[\mathbf{C_c}\right]^{-1} \cdot \left\{\mathbf{u_{B/A}}\right\} \tag{14}$$

From the equilibrium condition, relative displacements and Hooke's law, the following expressions are obtained:

$$\{P_1\ P_2 \ldots\ldots P_{11}\ P_{12}\}^T = \mathbf{\Pi} \cdot \{P_7\ P_8\ P_9\ P_{10}\ P_{11}\ P_{12}\}^T \tag{15}$$

$$\boldsymbol{u}_{B/A} = \mathbf{\Pi}^{\,T} \cdot \{u_1\ u_2\ \ldots\ldots\ u_{11}\ u_{12}\}^T \tag{16}$$

$$\{P_1\ P_2 \ldots\ldots P_{11}\ P_{12}\}^T = \mathbf{K}_c \cdot \{u_1\ u_2 \ldots\ldots u_{11}\ u_{12}\}^T \tag{17}$$

Finally, combining equations (10), (11), (12) and (13) the stiffness matrix of a cracked finite element yields:

$$\mathbf{K}_c = \mathbf{\Pi} \cdot \left(\mathbf{C}_c\right)^{-1} \cdot \mathbf{\Pi}^T \tag{18}$$

3.2. Equations of motion of the system

The vibrational behavior of an experimental rotor, as shown in Fig. 7, (including two spherical roller bearing, a rigid disk and a cracked shaft) is described by its equation of motion in stationary co-ordinates, Eq. (19), obtained by Nelson and Nataraj (1986) using finite element method. The shaft is modeled with five non-cracked finite elements and one cracked element. **M** is the mass matrix of the system; **D** is the viscous damping matrix; **G** is the gyroscopic matrix, **K**(*t*) is the stiffness matrix, ***F*(*t*)** is the force vector including the rotatory disk unbalance and the gravity load, and ***x*** is the displacement vector. It is assumed that the crack does not produce changes in the mass, gyroscopic and damping matrixes. The stiffness matrix varies with time due to opening and closing of the crack.

$$\mathbf{M}\ddot{\mathbf{x}} + \left[\mathbf{D} + \mathbf{G}\right]\dot{\mathbf{x}} + \mathbf{K}(\mathbf{t})\mathbf{x} = \mathbf{F}(\mathbf{t}) \tag{19}$$

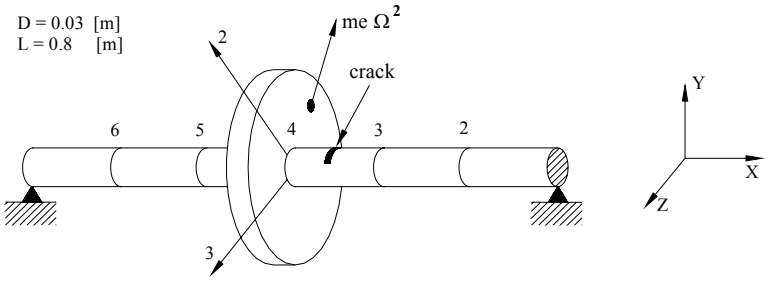

Figure 7. Rotor with a crack shaft model

The first step for evaluating **K**(*t*), is to determinate which part of the cracked section is opened at every time step. According to this, a great variety of models have been used. Jun and Eun (1992), and Gash (1993) utilize a switch model: crack completely opened or completely closed. Mayes and Davies (1984) and Huang et al. (1993) use a model that assume the stiffness variation as a continuous periodic function. Others investigators determine the instantaneous crack opening while the rotor is running, as the model proposed by Jun and Eun (1992), method that is used in this paper.

In this paper the theory of Jun and Eun (1992) is used, in order to calculate the additional flexibility coefficient of the cracked shaft. This procedure assumes that if the stress intensity factor has positive values there is a traction stress and, therefore the crack is open in the considered section. Otherwise, if $K_I<0$ it would be closed.

The flexibility coefficients C_{ij}^{1} are computed from the derivations discussed in reference by Dimarogonas and Paipetis (1983). The stiffness matrix of the cracked finite element, developed previously, is assembled with the other intact elements to obtain the global stiffness matrix.

The following is focused on the extraction of the vibrational behavior of the cracked rotor that is useful for crack identification. The currently vibration analyses used in the industry are primarily frequency spectra and waveforms measured at bearing supports

Figure 8 shows typical waterfall frequency spectra for radial directions of a perfectly balanced rotor containing a crack. The frequency at 1x, 2x and 3x rotor speed are due to the parametric vibrations induced by the crack. These spectra present components at the three first harmonics of the rotor speed 1xΩ, 2xΩ, 3xΩ, and their amplitudes will depend on how close they are to a critical speed

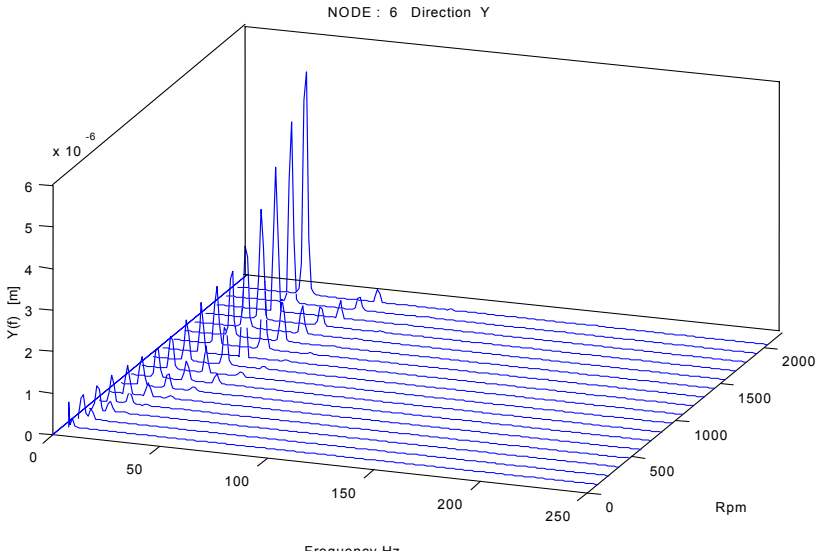

Figure 8 Node 6 frequency spectrum of an unbalanced cracked shaft-rotor.

However, this symptom is not a sufficient condition to detect this type of failure, as other common problems in rotating machines generate similar spectra, such as misalignment and casing distortion. For this reason it is necessary to use the vibrational spectrum and the waveform as a discriminator symptom for a cracked shaft. The authors of the present paper firmly believe that the analysis of the transient response of a rotor run-up and run-down will yield better diagnostic information than any other measure in steady state. During the transient operation, the various resonances of the system are excited and in this moment the particular nature of the problem is enhanced. So, the 2xΩ and 3xΩ components experience a peak and the orbits present, Fig. 9a, a typical form when the rotating speed coincides with 1/2 and 1/3 times the first critical speed, ω_1, since the orbit is very sensitive to any change in amplitude and phase relation between the spectral components.

3.3. Experimental results

The experimental testing ring of a motor, a flexible coupling and a single-disk rotor. A rotor shaft of 0.8 m in length, 0.03m in diameter, is supported by two identical spherical roller bearings. A disk of 0.22m in diameter and 0.04m in thickness is mounted on the rotor shaft mid-way between the bearing supports. A 1.5 kW a.c. motor drives the rotor-shaft. A variable frequency drive is used to vary the rotational speed from 0 to 1800 rpm. The shaft has a chordal crack localized at 0.04 m from the disk symmetry axe. The instrumentation used in the experiment includes non-

contacting displacement transducers, a phototacometer, four-channel digital recorder and a two-channel vibration analyzer.

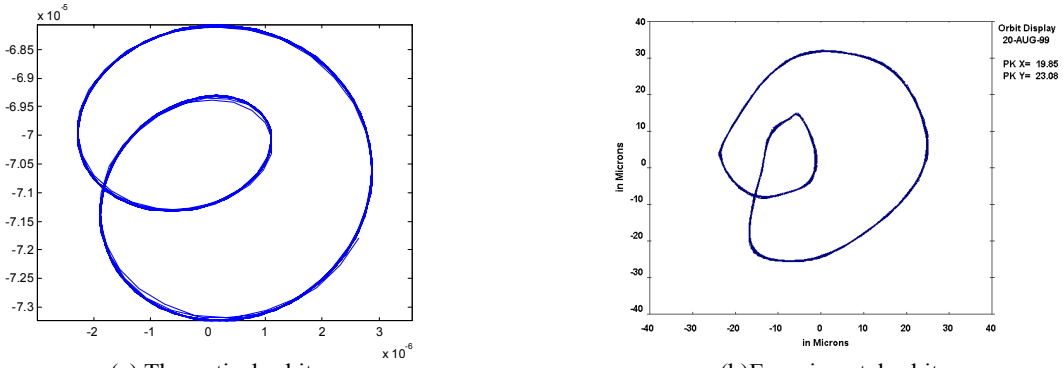

(a) Theoretical orbit (b)Experimental orbit

Figure 9. Orbit in node 6 at Ω=1194 rpm = 0.49ω_1

Figure 12 shows the results for a rotor with a crack of relative depth a/D=0.3, and the eccentricity of the unbalance mass e=0.18 mm. In the waterfall spectrum it is observe that the 2xΩ component experience a peak when the rotating speed coincide with ½ of the first natural frequency of the system, named sub-harmonic resonance. Some authors as Gash (1992) believe that this phenomenon can be used as a good indicator for crack identification. In addition, it is observe another characteristic that is an important indication of the existence of a crack. It is shown that for low rotational speed, when the unbalance effects are negligible, the vibration at 1xΩ is due to the crack.

The orbits measured and simulated for rotating speeds nearby the sub-harmonic resonance coincide, presenting a typical internal loop, which is a consequence of the magnification of the 2xΩ spectral component at that speed.

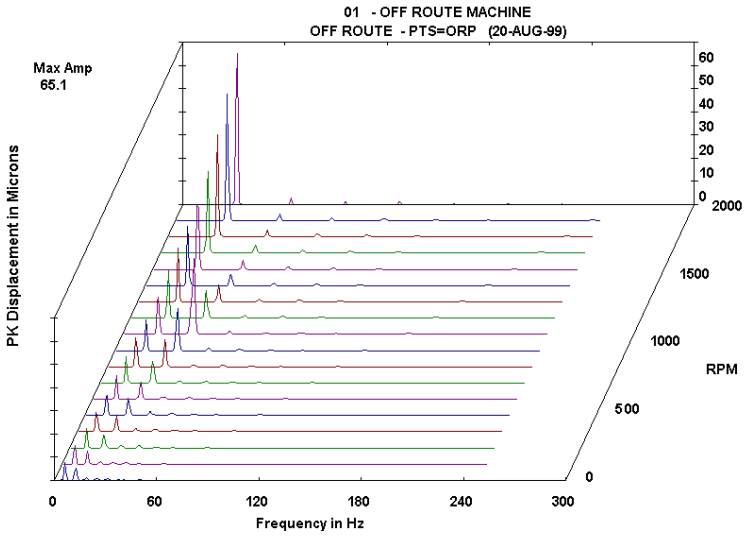

Figure 12. Node 6 experimental orbit and frequency spectrum of an unbalanced cracked shaft-rotor

From the previous analysis, the following characteristics symptom of a cracked rotor are drawn:

i) The 1xΩ, 2xΩ and 3xΩ spectral component, specially the two firsts and its relative amplitude will depend on the proximity that they have to a resonance or antiresonance.
ii) There are subharmonic resonances (peak in the response) when the rotating speed happened to be an integer fraction of the critical speed.
iii) The results showed that, for the best extraction of the signal information, the shaft should be run at one half of the first critical speed or acquire vibration signal during the rotor shutdown or startup.

Finally the model constructed here, is believed to provide a useful tool for the vibration analysis of any practical engineering rotor system.

4. Conclusions

From extensive theoretical simulations and experimental tests, the validity of the model proposed for the misaligned rotors of our paper has successfully verified. Our model allows us to explain the vibration behaviour of misaligned shafts connected through any type of flexible coupling. The vibration generated is of the parametric type, and it is caused by variation in the coupling stiffness as the shaft rotates. As a consequence, the vibration spectral response is directly related to the spectral coupling stiffness, *i.e*., it is strongly dependent upon the type of coupling used. Other factors on which the vibration spectrum depends include the system's frequency response functions, and the load transmitted by the flexible coupling.

The main characteristics of the vibration that misaligned shafts generate have been summarized and presented so that they may prove useful to field personnel that work in predictive maintenance. The traditional vibration analysis rules used in practical predictive maintenance to diagnose shaft misalignment have been evaluated. Previous works have indicated that the vibration spectra generated by shaft misalignment show many harmonics of the rotational speed, with the second order being the main spectral component. These works have tried to find a justification for this empirical rule, but with little success. In this work, we have shown that no "universal" rule for the identification of shaft misalignment in a vibration spectrum exists.

Using the theory of lineal fracture mechanics, the stiffness matrix of a cracked shaft finite element was developed. This element can be used in a standard finite element program in order to analyze the static, dynamic and stability behavior of different structures.

5. Acknowledgements

The authors would like to acknowledge the FONDECYT of Chile, project Nº1030323 for the support of this work.

6. References

Dimarogonas, A. D. and Paipetiis, S. A., 1983, "Analytical Methods in Rotor Dynamic", Applied Science, London.

Gash, R., 1993, "A survey of the dynamic behavior of a simple rotor shaft with a transverse crack", Journal of Sound and Vibration, Vol.62, Nº2, pp.313-332

Gibbons, C.B., 1976,"Coupling misalignment forces", Proceedings of the Fifth Turbomachinery Symposium, Gas Turbine Laboratories, Texas A & M University, College Station, Texas, pp. 111-116.

Huang, S. C., Huanh, Y. M., and Shieh, S. M., 1993, "Vibration and stability of a rotating shaft containing a transverse crack", Journal of Sound and Vibration, Vol. 162, Nº2, pp. 387-401.

Jun, O.S. and Eun, H. J., 1992, "Modeling and vibration analysis of a simple rotor with a breathing crack", Journal of Sound and Vibration, Vol. 155, Nº2, pp. 273-290.

Mayes, I. W. and Davies, W. G. R., 1984, "Analysis of the response of a multi-rotor bearing system containing a transverse crack in a rotor" ASME Journal of Vibration, Acoustics, Stress and Reliability in Design, Vol. 106, pp.139-145.

Nelson, H. D. and Nataraj, C., 1986, "The dynamic of a rotor system with a cracked shaft", ASME Journal of Vibration, Acoustics, Stress and Reliability in Design, Vol. 108, pp.189-196.

Piotrowski, J., 1986 Shaft Alignment Handbook. New York and Basle: Marcel Dekker, Inc.

Ramírez, D.E., 2003, "Análisis del comportamiento vibratorio de máquinas rotatorias". Master Thesis, Universidad de Concepción, Chile.

Saavedra, P., Baquedano, D., and San Juan, L., 1996, "Modelo numérico para el estudio dinámico de un rotor con eje agrietado", Revista Internacional de Métodos Numéricos para Cálculo y Diseño en Ingeniería, Vol. 12,pp. 125-146.

Xu, M. and Marangoni R.D., 1994, "Vibration analysis of a motor-flexible coupling-rotor system subject to misalignment and unbalance, part I: theoretical model and analysis". Journal of Sound and Vibration, ,Vol. 176, Nº5, pp. 663-679.

7. Responsibility notice

The authors are the only responsible for the printed material included in this paper.